INTERNATIONAL JOURNAL FOR NUMERICAL METHODS IN FLUIDS
Int. J. Numer. Meth. Fluids 2009; **60**:867–891
Published online 20 October 2008 in Wiley InterScience (www.interscience.wiley.com). DOI: 10.1002/fld.1903

Multicomponent dissipative particle dynamics: Formulation of a general framework for simulations of complex fluids

Anuj Chaudhri and Jennifer R. Lukes*, †

Department of Mechanical Engineering and Applied Mechanics, University of Pennsylvania, Philadelphia, PA 19104, U.S.A.

SUMMARY

The dissipative particle dynamics mesoscopic simulation method is analyzed thoroughly by identifying the scaling factors necessary to simulate a multicomponent system. A new framework of general expressions is derived relating the parameters in the system to their dimensionless quantities. The consistent non-dimensionalization used in this paper serves to connect the previous models in the literature. When the scaling factors are based on the solvent in a multicomponent system, the system of equations reduces to the well-known Groot and Warren model. Validation results for ideal, simple and binary immiscible fluids are presented and compared with established results from the literature. The framework established herein is an important step toward the practical application of dissipative particle dynamics for the analysis of complex fluid systems. Copyright © 2008 John Wiley & Sons, Ltd.

Received 22 October 2007; Revised 9 July 2008; Accepted 13 July 2008

KEY WORDS: dissipative particle dynamics; particle methods; complex fluids; multicomponent; dimensional analysis

1. INTRODUCTION

Complex fluids are examples of soft condensed matter systems that are ubiquitous in nature [1]. Paints, emulsions, gels, sols, polymeric liquids, liquid crystals, lubricants, foods and common fluids such as blood and tap water are complex fluids. A complex fluid is defined as a fluid with suspended particles, droplets, bubbles, micelles or vesicles, whose characteristic size is in the mesoscopic domain, i.e. a few nanometers to a few microns [2]. The mesoscopic structure of the

*Correspondence to: Jennifer R. Lukes, Department of Mechanical Engineering and Applied Mechanics, 220 South 33rd Street, University of Pennsylvania, Philadelphia, PA 19104, U.S.A.
†E-mail: jrlukes@seas.upenn.edu

Contract/grant sponsor: NSF NSEC; contract/grant number: DMR-0425780
Contract/grant sponsor: Office of Naval Research; contract/grant number: N00014-07-1-0665

fluid leads to unusual static and dynamic properties observed at the macroscale. For example, the macroscale mechanical properties of complex fluids are intermediate between classical solids and liquids [3].

Most methods for understanding the physical properties and calculating the dynamic response are based on incorporating non-Newtonian behavior in the continuum Navier–Stokes equations of fluid mechanics [4, 5]. These methods have shown very good agreement with experiments for simple colloidal Brownian suspensions, where particle sizes are much bigger than the corresponding solvent and the effect of the solvent can be averaged out. For systems with smaller particle sizes, however, this averaging is not applicable and the microstructure can have a significant effect on the dynamic response. Important contributions to the dynamic response come not only from the hydrodynamic description of the system but also from the thermal fluctuations at mesoscopic scales, which affect the macroscopic equilibrium and non-equilibrium transport properties of the system. Continuum methods are inadequate in this regard and hence there is a need to develop models that are more fundamental in nature.

The most fundamental method that models fluids from a microscopic, deterministic perspective is molecular dynamics (MD) [6, 7], which tracks individual atomic motion to calculate fluid properties and behavior. Any system that needs to be modeled from an atomistic or molecular point of view with thermal fluctuations could in principle be modeled with MD. The time and length scales that can be probed with MD have limits in the nanoscopic domain and need very large system sizes and long runs to reach the hydrodynamic regime. This requires tremendous computing power, which is often not readily available. In addition, mesoscale length and time scales cannot be probed easily with MD.

Over the years there has been much interest in developing methods that model fluid systems at the mesoscale level. In mesoscopic systems, the fastest atomistic length and time scales commonly treated by methods such as MD are coarse grained in order to be able to treat the larger length and time scales of interest in these systems. Some of these methods include Brownian dynamics (BD) [8], dissipative particle dynamics (DPD) [9], Stokesian dynamics [10], smoothed DPD [11], lattice Boltzmann [12] and lattice gas automata [13]. Particle-based methods are simple to implement and do not suffer from problems associated with grids or lattices. Boundary conditions are also easier to apply and a wide variety of fluids and mixtures can be modeled as long as inter- and intra-particle interactions are known [14].

DPD is a meshless, coarse-grained, particle-based simulation method used to simulate systems at mesoscopic length and time scales. It can be thought of as a coarse-grained version of MD with soft inter-particle forces between groups of molecules called beads. The DPD method has shown tremendous potential for modeling systems where hydrodynamic forces are important. In addition to the soft interactions, dissipative and random forces are added, which together act as a thermostat and keep the system in equilibrium. This makes DPD a very attractive scheme as it models the solvent explicitly and includes the hydrodynamic interactions that are absent from BD simulations. The method also conserves both linear and angular momentum as all the interaction forces are pairwise in nature and act between molecular centers. The factor of 1000 time step increase and the factor of 10–100 size scale increase [15] over MD enable the treatment of realistic systems at length scales up to tens of microns and time scales up to hundreds of microseconds on a single processor. The model is isotropic, Galilean invariant and can be interpreted as a Lagrangian discretization to the equations of fluctuating hydrodynamics as the particles flow and exhibit thermal fluctuations. It has been used to model Couette flow through a square array of cylinders [9], lipid bilayer membranes [16–18], vesicles [19], mesophage formation

DOI: 10.1002/fld

and behavior [20], polymersomes [21], binary immiscible fluids [15, 22], colloidal suspensions [23], nanotube–polymer composites [24] and polymer solutions [25].

Despite the fact that significant progress has been made in applying DPD to model single and multicomponent systems, a consistent, general framework has not been established. The previous models only work for parameter choices based on water as a solvent. Additionally, all the DPD beads have traditionally been assumed to have equal volumes with three water molecules assigned per bead. This restricts the usefulness of DPD in representing multicomponent complex structures where the bead sizes could vary over the different components or where the solvent is no longer water-based. Hence, developing a framework with no such restrictions is necessary to enable exploration of a large variety of systems. In this paper, we tackle this issue by writing dimensional equations of motion that can be used for any multicomponent DPD model. We then nondimensionalize these equations and explicitly define scaling factors that are consistent with standard DPD practice. When the scaling factors are based on the solvent in a multicomponent system, the multicomponent equations derived herein reduce to the Groot/Warren equations used most often in the literature. Validation results for ideal, simple and binary immiscible DPD fluids are then presented and compared with published results.

2. GENERAL DPD EQUATIONS

A complex fluid has many degrees of freedom when viewed from a microscopic (atomistic) perspective. Coarse-graining reduces the number of degrees of freedom by eliminating 'irrelevant' variables—variables not required for the accurate calculation of macroscopic physical properties of the system. The state of the system at the coarse-grained level is then described by a smaller set of 'relevant' variables. In this way coarse-graining should be done so that the faster degrees of freedom are removed in favor of the slowly varying ones. Of all the possible levels of description of a system, two of them have been very well studied: (1) microscopic and (2) macroscopic or thermodynamic [26]. The microscopic level is governed by the classical Newtonian or Hamiltonian equations of motion. The macroscopic level is governed by the laws of equilibrium thermodynamics. Levels in between are governed by kinetic equations that follow after the elimination of variables. Microscopically, the state of a system is described by the positions and momenta of the individual atoms. If the atoms are grouped together in clusters so that the motion of the center of mass of clusters is tracked by the position and momentum variables $\{\mathbf{r}, \mathbf{p}\}$, then the dynamics of this mesoscale level of description is described by a set of evolution equations for $\{\mathbf{r}, \mathbf{p}\}$. If the time scales at which the system evolves microscopically are clearly separable from the time scales at which the variables $\{\mathbf{r}, \mathbf{p}\}$ of the mesoscale evolve, the evolution equations of the coarse-grained level are Markovian, i.e. the history of the system is not important to determine the future state. In addition, since some variables have been eliminated at the coarse-grained level, information regarding the initial microstate is missing. Many microstates could possibly give the same 'mesostate'. This uncertainty in the initial state creates an uncertainty in the evolution of the coarse-grained state. This leads to a stochastic description of the system and the problem can be mapped to a set of stochastic differential equations. Hence, all mesoscopic methods are based on a statistical description of the distribution of random variables. In the case described above, $\{\mathbf{r}, \mathbf{p}\}$ are the random variables that govern the mesoscopic dynamics. The evolution equations for $\{\mathbf{r}, \mathbf{p}\}$ are of the Langevin type with drift and diffusion terms [27]. Equivalently, the probability distribution function of these random variables can also be used to describe the system and the corresponding

DOI: 10.1002/fld

equations would be of the Fokker–Planck type, which are mathematically equivalent to a set of stochastic differential equations.

The DPD equations of motion are stochastic ordinary differential equations of the Langevin type. In this paper the mesoscopic clusters of atoms, molecules or monomers that are modeled with DPD forces will be called beads and the individual atoms/molecules/monomers that make up the bead will be referred to as particles. Hence, a mesoscopic DPD bead is made up of many microscopic particles. Given a set of beads the state of the mesoscopic system is described by the bead position and momentum coordinates $\{\mathbf{r}, \mathbf{p}\}$. The position and momentum coordinates are treated as random variables at this level of description of the system. The time scale of evolution of these variables is clearly separated from the fast molecular vibrations of the atomic bonds, which makes the description Markovian. If X represents a random variable that evolves from a time t to a time $t+\mathrm{d}t$, then continuous time Markovian processes evolve with the following type of Langevin equation [28]:

$$X(t+\mathrm{d}t) = X(t) + A(X(t), t)\,\mathrm{d}t + [D(X(t), t)]^{1/2}\,\mathrm{d}t^{1/2} N(0, 1) \tag{1}$$

where $A(X(t), t)$ is the drift term, $D(X(t), t)$ where $D \geqslant 0$ is the diffusion term and $N(0, 1)$ is a normal random variable with zero mean and unit variance. Equation (1) indicates that any continuous Markov process could be expressed as a linear combination of normal random variables. If the variables $A(X(t), t)$ and $D(X(t), t)$ are constant, then Equation (1) reduces to a completely homogeneous Markov process known as the Weiner process W. The Weiner process is frequently used to model diffusive behavior in physical systems:

$$X(t+\mathrm{d}t) = X(t) + A\,\mathrm{d}t + D^{1/2}\,\mathrm{d}W \tag{2}$$

$$\mathrm{d}W = N(0, \mathrm{d}t) = N(0, 1)\,\mathrm{d}t^{1/2} \tag{3}$$

The transformation to a unit normal random variable in Equation (3) can be derived in a simple way using concepts of probability theory [29]. In the case of DPD, the momenta $\mathbf{p}$ of the beads have the same form as Equation (2). The positions are updated from these momenta. The momentum variables are propagated based on forces that are generally divided into three kinds: conservative, dissipative and random. The dissipative forces are related to the drift term A in Equation (2) and the random forces are related to the diffusive forces modeled by the Weiner process. The dissipative and random forces are consequences of the degrees of freedom 'lost' or coarse-grained during the averaging process and lead to fluctuations of the bead velocity, which can be intuitively understood to arise from the fact that there can be particle exchange between beads (keeping the total number of particles constant). The dissipative forces in the system spread the energy of the system and help in lowering the temperature of the system. The random forces tend to heat the system and in tandem with the dissipation maintain the temperature of the system. Hence, the DPD algorithm provides a natural thermostat. It has been shown theoretically [30–32] that the equilibrium probability distribution of the evolution of the position and momentum variables is Gaussian for continuous time DPD, which means that the temperature of the system will remain constant in the theoretical limit of zero time step. However, for the finite time version, the temperature of the system is a function of the time step due to discretization errors, where the random and dissipative forces are assumed to be constant over the time step. The conservative forces between beads model the chemistry and represent the pressure forces in the system.

Let us consider a system of N beads in a simulation box of volume Ω. Let N_α denote the number of beads corresponding to the component α in the system. By component we mean a type

DOI: 10.1002/fld

of species in the multicomponent system, for example, oil in a water–oil system. Each bead of the component has a volume Φ_α and has a mass m_α. The coarse-graining determines the number of particles N_α^m in each bead:

$$m_\alpha = N_\alpha^m \cdot m_\alpha^{\text{particle}} \tag{4}$$

$$\Phi_\alpha = N_\alpha^m \cdot \Phi_\alpha^{\text{particle}} \tag{5}$$

$m_\alpha^{\text{particle}}$ and $\Phi_\alpha^{\text{particle}}$ are the mass and volume, respectively, of the particles that make up the DPD bead. The dimensionless number density $\bar{\rho}_\alpha$ is defined as the number of beads that can fill a cubic box of side length $r_{\alpha,\alpha}^{\text{c}}$:

$$[r_{\alpha,\alpha}^{\text{c}}]^3 = \bar{\rho}_\alpha \Phi_\alpha \tag{6}$$

$r_{\alpha,\alpha}^{\text{c}}$ represents the cut-off radius: the distance beyond which the DPD beads of component α do not interact. A good definition for inter-component cut-off radius $r_{\alpha,\beta}^{\text{c}}$, where β represents another component in the fluid, is not available. However, to make the simulations simpler, we make the assumption that $r_{\alpha,\beta}^{\text{c}}$ is given by the arithmetic mean of $r_{\alpha,\alpha}^{\text{c}}$ and $r_{\beta,\beta}^{\text{c}}$.

In case of a multicomponent system, the total number of beads and the total volume of the system are given as

$$N = \sum_\alpha N_\alpha \tag{7}$$

$$\Omega = \sum_\alpha \Omega_\alpha \tag{8}$$

The volume Ω_α of component α is given by the product of the number of beads N_α and the volume of each bead Φ_α. Hence, Equation (8) for the total volume of the system becomes

$$\Omega = \sum_\alpha N_\alpha \Phi_\alpha \tag{9}$$

Equation (6) can be used to calculate the simulation box volume:

$$\Omega = \sum_\alpha N_\alpha \frac{[r_{\alpha,\alpha}^{\text{c}}]^3}{\bar{\rho}_\alpha} \tag{10}$$

The equations of motion for the ith bead of component α with position coordinates $\mathbf{r}_{i\alpha}$ and velocity vector $\mathbf{v}_{i\alpha}$ can be expressed as

$$\frac{\mathrm{d}}{\mathrm{d}t}[\mathbf{r}_{i\alpha}] = \mathbf{v}_{i\alpha} \tag{11}$$

$$m_\alpha \frac{\mathrm{d}}{\mathrm{d}t}[\mathbf{v}_{i\alpha}] = \mathbf{F}_{i\alpha}^{\text{C}} + \mathbf{F}_{i\alpha}^{\text{D}} + \mathbf{F}_{i\alpha}^{\text{R}} \tag{12}$$

where $\mathbf{F}_{i\alpha}^{\text{C}}$, $\mathbf{F}_{i\alpha}^{\text{D}}$ and $\mathbf{F}_{i\alpha}^{\text{R}}$ are the conservative, dissipative and random forces acting on the ith bead of component α. Following Coveney and Español [33] the forces can be defined in the following

DOI: 10.1002/fld

manner:

$$\mathbf{F}^{\mathrm{C}}_{i\alpha}=\sum_{\beta}\sum_{j\beta\neq i\alpha}^{N_\beta}\mathbf{f}^{\mathrm{C}}_{i\alpha,j\beta} \tag{13}$$

$$\mathbf{f}^{\mathrm{C}}_{i\alpha,j\beta}=a_{\alpha,\beta}\,w^{\mathrm{C}}_{i\alpha,j\beta}(r_{i\alpha,j\beta})\hat{\mathbf{r}}_{i\alpha,j\beta} \tag{14}$$

$$\mathbf{F}^{\mathrm{D}}_{i\alpha}=-\sum_{\beta}\sum_{j\beta\neq i\alpha}^{N_\beta}\mathbf{f}^{\mathrm{D}}_{i\alpha,j\beta} \tag{15}$$

$$\mathbf{f}^{\mathrm{D}}_{i\alpha,j\beta}=\gamma_{\alpha,\beta}w^{\mathrm{D}}_{i\alpha,j\beta}(r_{i\alpha,j\beta})\,[\mathbf{v}_{i\alpha,j\beta}\cdot\hat{\mathbf{r}}_{i\alpha,j\beta}]\hat{\mathbf{r}}_{i\alpha,j\beta} \tag{16}$$

$$\mathbf{F}^{\mathrm{R}}_{i\alpha}=\sum_{\beta}\sum_{j\beta\neq i\alpha}^{N_\beta}\mathbf{f}^{\mathrm{R}}_{i\alpha,j\beta} \tag{17}$$

$$\mathbf{f}^{\mathrm{R}}_{i\alpha,j\beta}=\sigma_{\alpha,\beta}w^{\mathrm{R}}_{i\alpha,j\beta}(r_{i\alpha,j\beta})\,\xi_{i\alpha,j\beta}\hat{\mathbf{r}}_{i\alpha,j\beta} \tag{18}$$

In Equations (13), (15) and (17), the index β runs over all components and $a_{\alpha,\beta}$, $\gamma_{\alpha,\beta}$, $\sigma_{\alpha,\beta}$ are the conservative, dissipative and random force parameters between beads i and j of components α and β, respectively. The conservative parameter $a_{\alpha,\beta}$ has units of force, the dissipative parameter $\gamma_{\alpha,\beta}$ has units of force per unit velocity and the random noise parameter $\sigma_{\alpha,\beta}$ has units of force$*$(time)$^{1/2}$. $w_{i\alpha,j\beta}$ is an arbitrary weight function that vanishes at $r_{i\alpha,j\beta}=r^{\mathrm{c}}_{\alpha,\beta}$. The position, dimensionless position and relative velocity vectors between beads $i\alpha$ and $j\beta$ are defined as

$$\mathbf{r}_{i\alpha,j\beta}=\mathbf{r}_{i\alpha}-\mathbf{r}_{j\beta} \tag{19}$$

$$\hat{\mathbf{r}}_{i\alpha,j\beta}=\frac{\mathbf{r}_{i\alpha,j\beta}}{r_{i\alpha,j\beta}} \tag{20}$$

$$\mathbf{v}_{i\alpha,j\beta}=\mathbf{v}_{i\alpha}-\mathbf{v}_{j\beta} \tag{21}$$

and the magnitude of the position vector is given as

$$r_{i\alpha,j\beta}=|\mathbf{r}_{i\alpha,j\beta}| \tag{22}$$

The conservative and random weight functions in Equations (14) and (18) are of a form used previously [34]

$$w_{i\alpha,j\beta}(r_{i\alpha,j\beta})=\begin{cases}1-\dfrac{r_{i\alpha,j\beta}}{r^{\mathrm{c}}_{\alpha,\beta}}, & r_{i\alpha,j\beta}\leqslant r^{\mathrm{c}}_{\alpha,\beta}\\ 0, & r_{i\alpha,j\beta}>r^{\mathrm{c}}_{\alpha,\beta}\end{cases} \tag{23}$$

which gives the beads a soft repulsive character. The dissipative weight function is defined later in Equation (30).

The random force term in Equation (18) is governed by the randomly fluctuating quantity $\xi_{i\alpha,j\beta}$, which obeys Gaussian statistics due to its Markovian character. $\xi_{i\alpha,j\beta}$ is generally taken to be

DOI: 10.1002/fld

a delta correlated distribution with zero mean

$$\langle \xi_{i\alpha,j\beta}(t) \rangle = 0 \tag{24}$$

delta variance

$$\langle \xi_{i\alpha,j\beta}(t) \xi_{k\alpha,l\beta}(t') \rangle = \langle \delta_{i\alpha,k\alpha}(t) \delta_{j\beta,l\beta}(t) + \delta_{i\alpha,l\beta}(t) \delta_{j\beta,k\alpha}(t) \rangle \delta(t-t') \tag{25}$$

and symmetry [30]

$$\xi_{i\alpha,j\beta} = \xi_{j\beta,i\alpha} \tag{26}$$

The symmetry property ensures that the total momentum of the system is conserved. Equation (25) indicates that at times $t = t'$, the random forces between two distinct bead pairs $(i\alpha, j\beta)$ and $(k\alpha, l\beta)$ will be uncorrelated. At all other times, the delta function is identically zero. Equation (25) is the most general way of defining the delta-correlated random term as it includes the straight (intra-component) and cross correlation (inter-component) terms between particle pairs.

To implement the random force as given in Equation (18) numerically, the properties of the random variable $\xi_{i\alpha,j\beta}$ have to be known. Groot/Warren [34] and Español/Warren [30] have shown that the noise term $\xi_{i\alpha,j\beta}$ can be interpreted as the time derivative of the Weiner process, which from Equation (3) is just a normal random variable of order $\mathrm{d}t^{1/2}$:

$$\xi_{i\alpha,j\beta} = \frac{\mathrm{d}W}{\mathrm{d}t} = \frac{N(0,1)\,\mathrm{d}t^{1/2}}{\mathrm{d}t} = N(0,1)\,\mathrm{d}t^{-1/2} \tag{27}$$

For computer simulations, the normal random variable $N(0,1)$ becomes a normal random number $\psi_{i\alpha,j\beta}$ with zero mean and unit variance and is chosen independently for every pair of interacting beads in the system. Substituting Equation (27), Equation (18) becomes

$$\mathbf{f}^{\mathrm{R}}_{i\alpha,j\beta} = \sigma_{\alpha,\beta} w^{\mathrm{R}}_{i\alpha,j\beta}(r_{i\alpha,j\beta})\, \psi_{i\alpha,j\beta}\, \mathrm{d}t^{-1/2}\, \hat{\mathbf{r}}_{i\alpha,j\beta} \tag{28}$$

All the forces are pairwise in nature and hence help conserve linear and angular momentum. Any additional forces in the system such as spring or bond angle forces can be added to the beads to simulate a solid-like or soft-particle system [35].

In order to make the stochastic differential equations in (11) and (12) work for a given system at thermal equilibrium, the fluctuation–dissipation (FD) theorem and the detailed balance conditions have to be satisfied. These conditions ensure that the system Hamiltonian has a Gibbsian canonical equilibrium distribution. Español/Warren [30] derived the conditions for the Gibbsian equilibrium from the equivalent Fokker–Planck equation. Later Marsh *et al.* [31] confirmed that this is indeed the case and if the detailed balance is not satisfied, then the Gibbs state is not a stationary state of the system and thermal equilibrium can never be obtained. This constant temperature version of DPD does not have a corresponding energy equation and hence energy is not conserved in the system. In accordance with the above considerations, the following conditions need to be satisfied for the multicomponent constant temperature version of DPD [33]:

$$\sigma^2_{\alpha,\beta} = 2\gamma_{\alpha,\beta} k_B T \tag{29}$$

$$w^{\mathrm{D}}_{i\alpha,j\beta}(r_{i\alpha,j\beta}) = [w^{\mathrm{R}}_{i\alpha,j\beta}(r_{i\alpha,j\beta})]^2 \tag{30}$$

DOI: 10.1002/fld

3. DIMENSIONLESS DPD EQUATIONS

In DPD, the governing equations are typically expressed in dimensionless form. To relate DPD simulation results to real physical quantities, scaling factors linking dimensional and dimensionless quantities must be identified. Although scale factors for quantities such as mass, length, and thermal energy have been defined previously [34], scale factors for other quantities have not been explicitly defined. This makes it unclear as to how to compute dimensional physical properties in DPD. Here we find explicit definitions for the unknown scale factors following a two step process. First, in this section, we nondimensionalize the DPD expressions from Section 2 using general scale factors (denoted with asterisks) that have not yet been defined in terms of the known parameters of the system. Then in Section 4 we compare the resultant equations to standard DPD equations in the literature to explicitly define scaling factors that are consistent with standard DPD practice.

Nondimensionalization by scaling factors is often used to reduce the number of independent parameters in the governing equations and thus simplify their solution. In fluid mechanics, for example, nondimensionalization of the variables of the problem leads to dimensionless equations of motion and well known dimensionless groupings of parameters such as the Reynolds number. In contrast, the dimensionless equations of DPD have the same number of parameters as the dimensional equations of motion. Reduction in the number of parameters does not occur in DPD for two reasons. First, according to DPD convention, *all* parameters, including variables and material parameters, are scaled. In fluid mechanics, material parameters such as density and viscosity are not typically scaled. Additionally, the conventional DPD scaling is such that the dimensionless values of several material parameters are not equal to one. For example, the dimensionless conservative and random force parameters commonly assume the values 25 (assuming one water molecule per bead) and 3, respectively, for water at room temperature [34]. Hence, dimensionless material parameters appear individually in the nondimensional DPD equations, in contrast to fluid mechanics where dimensional parameters are grouped into dimensionless quantities. The lack of grouping in DPD is why there is no reduction in the number of parameters.

Proper definition of scaling factors depends on the dominant physics of each particular system and can vary depending on the type of problem. In fluid mechanics, the appropriate pressure scaling is different for high and low speed flows, depending on dynamic pressure and viscous stress, respectively [36]. As the appropriate scale factors are not necessarily the same or known *a priori*

Table I. Dimensionless quantities and scaling factors for parameters used in the DPD system.

Length	$\bar{\mathbf{r}}=\mathbf{r}/r^*$
Velocity	$\bar{\mathbf{v}}=\mathbf{v}/v^*$
Time	$\bar{t}=t/t^*$
Mass	$\bar{m}=m/m^*$
Force	$\bar{\mathbf{F}}=\mathbf{F}/F^*$
Conservative force parameter	$\bar{a}=a/a^*$
Dissipative force parameter	$\bar{\gamma}=\gamma/\gamma^*$
Random force parameter	$\bar{\sigma}=\sigma/\sigma^*$
Thermal energy*	$\overline{k_BT}=k_BT/[k_BT]^*$
System volume	$\bar{\Omega}=\Omega/\Omega^*$

*Note that the same definition applies to temperature as k_B is a constant.

DOI: 10.1002/fld

for every DPD problem, we follow Munson *et al.* [37] and nondimensionalize the governing equations using *general* scaling factors (denoted with asterisks) that have *not yet been defined* in terms of the known parameters of the system. In Section 4 we explicitly define the scaling factors. These scaling factors are the DPD units that are used in the simulations. For example, length is measured in units of r^*, velocity in units of v^* and time in units of t^*. The resultant dimensionless parameters are denoted with an overbar as shown in Table I.

With the above definitions for dimensionless quantities, the system volume in Equation (10) reduces to the following dimensionless expression:

$$\bar{\Omega}=\left[\frac{[r^*]^3}{\Omega^*}\right]\left[\sum_\alpha N_\alpha \frac{[\bar{r}^{\mathrm{c}}_{\alpha,\alpha}]^3}{\bar{\rho}_\alpha}\right] \tag{31}$$

On replacing the dimensional variables in Equations (11) and (12) with the dimensionless variables defined in Table I, the equations of motion for the ith particle of component α transform as

$$\frac{\mathrm{d}}{\mathrm{d}\bar{t}}[\bar{\mathbf{r}}_{i\alpha}]=\left[\frac{v^*t^*}{r^*}\right]\bar{\mathbf{v}}_{i\alpha} \tag{32}$$

$$\bar{m}_\alpha\frac{\mathrm{d}}{\mathrm{d}\bar{t}}[\bar{\mathbf{v}}_{i\alpha}]=\left[\frac{F^*t^*}{m^*v^*}\right][\bar{\mathbf{F}}^{\mathrm{C}}_{i\alpha}+\bar{\mathbf{F}}^{\mathrm{D}}_{i\alpha}+\bar{\mathbf{F}}^{\mathrm{R}}_{i\alpha}] \tag{33}$$

The weight function used most commonly for soft repulsive forces is dimensionless and has the same form as Equation (23):

$$\bar{w}_{i\alpha,j\beta}(\bar{r}_{i\alpha,j\beta})=\begin{cases}1-\dfrac{\bar{r}_{i\alpha,j\beta}}{\bar{r}^{\mathrm{c}}_{\alpha,\beta}}, & \bar{r}_{i\alpha,j\beta}\leqslant\bar{r}^{\mathrm{c}}_{\alpha,\beta}\\ 0, & \bar{r}_{i\alpha,j\beta}>\bar{r}^{\mathrm{c}}_{\alpha,\beta}\end{cases} \tag{34}$$

Similarly, the dimensionless counterparts of Equations (13)–(17) and (28)–(30) are

$$\bar{\mathbf{F}}^{\mathrm{C}}_{i\alpha}=\sum_\beta\sum_{j\beta\neq i\alpha}^{N_\beta}\bar{\mathbf{f}}^{\mathrm{C}}_{i\alpha,j\beta} \tag{35}$$

$$\bar{\mathbf{f}}^{\mathrm{C}}_{i\alpha,j\beta}=\left[\frac{a^*}{F^*}\right]\bar{a}_{\alpha,\beta}\bar{w}^{\mathrm{C}}_{i\alpha,j\beta}(\bar{r}_{i\alpha,j\beta})\hat{\bar{\mathbf{r}}}_{i\alpha,j\beta} \tag{36}$$

$$\bar{\mathbf{F}}^{\mathrm{D}}_{i\alpha}=-\sum_\beta\sum_{j\beta\neq i\alpha}^{N_\beta}\bar{\mathbf{f}}^{\mathrm{D}}_{i\alpha,j\beta} \tag{37}$$

$$\bar{\mathbf{f}}^{\mathrm{D}}_{i\alpha,j\beta}=\left[\frac{\gamma^*v^*}{F^*}\right]\bar{\gamma}_{\alpha,\beta}\bar{w}^{\mathrm{D}}_{i\alpha,j\beta}(\bar{r}_{i\alpha,j\beta})\,[\bar{\mathbf{v}}_{i\alpha,j\beta}\cdot\hat{\bar{\mathbf{r}}}_{i\alpha,j\beta}]\hat{\bar{\mathbf{r}}}_{i\alpha,j\beta} \tag{38}$$

$$\bar{\mathbf{F}}^{\mathrm{R}}_{i\alpha}=\sum_\beta\sum_{j\beta\neq i\alpha}^{N_\beta}\bar{\mathbf{f}}^{\mathrm{R}}_{i\alpha,j\beta} \tag{39}$$

$$\bar{\mathbf{f}}^{\mathrm{R}}_{i\alpha,j\beta}=\left[\frac{\sigma^*}{F^*[t^*]^{1/2}}\right]\bar{\sigma}_{\alpha,\beta}\bar{w}^{\mathrm{R}}_{i\alpha,j\beta}(\bar{r}_{i\alpha,j\beta})\bar{\psi}_{i\alpha,j\beta}\,\mathrm{d}\bar{t}^{-1/2}\hat{\bar{\mathbf{r}}}_{i\alpha,j\beta} \tag{40}$$

DOI: 10.1002/fld

$$\bar{\sigma}^2_{\alpha,\beta} = \left[\frac{\gamma^*[k_BT]^*}{[\sigma^*]^2}\right] 2\bar{\gamma}_{\alpha,\beta}\overline{k_BT} \tag{41}$$

$$\bar{w}^{\mathrm{D}}_{i\alpha,j\beta}(\bar{r}_{i\alpha,j\beta}) = [\bar{w}^{\mathrm{R}}_{i\alpha,j\beta}(\bar{r}_{i\alpha,j\beta})]^2 \tag{42}$$

The equations of motion (32) and (33) define an initial value problem and can be solved with two initial conditions. The initial positions and initial velocities are specified and the equations propagated in time using special integrators. The initial velocity is set using the equipartition theorem to set the thermal energy $\overline{k_BT}$:

$$\frac{1}{2}\sum_i \bar{m}_\alpha \bar{\mathbf{v}}^2_{i\alpha} = \frac{3}{2}\left[\frac{[k_BT]^*}{m^*[v^*]^2}\right] N_\alpha \overline{k_BT} \tag{43}$$

The kinetic temperature of the system can be calculated at any point in the simulation by inverting the expression in Equation (43).

4. EXPLICIT DEFINITION OF SCALING FACTORS FOR MULTICOMPONENT DPD EQUATIONS

The model of Groot/Warren explicitly defined scaling factors for mass, length, and thermal energy but did not do so for several other important quantities in Table I. In this section we explicitly define the remaining scaling factors in a manner consistent with this model. This is done by first recalling the velocity and time scaling factors of Ripoll *et al.* [38] and then by comparing the dimensionless equations of Section 3 to the Groot/Warren model. It is shown that the square bracketed prefactor groupings of general scaling factors in Equations (31)–(33), (36), (38), (40), (41), and (43) must reduce to one to recover the Groot/Warren model. The scaling factors are generalized to multicomponent systems and are based on the solvent, which has faster time scales compared with the suspended particles or monomers in such systems. The solvent component is denoted by the subscript (1) and solvent–solvent interactions are denoted by the subscript $(1,1)$.

Following Groot/Warren, the scaling factor for mass is the mass of the solvent

$$m^* = m_{(1)} \tag{44}$$

the scaling factor for length is the cut-off distance for the solvent–solvent interaction

$$r^* = r^{\mathrm{c}}_{(1,1)} \tag{45}$$

and the thermal energy scale is the thermal energy of the solvent

$$[k_BT]^* = [k_BT] \tag{46}$$

Following Ripoll *et al.* [38], the thermal velocity of the solvent particle is chosen as the velocity scale

$$v^* = \sqrt{\frac{[k_BT]}{m_{(1)}}} \tag{47}$$

DOI: 10.1002/fld

and the time scale is set as the traversal time. This time, which is defined as a ratio of the solvent–solvent cut-off distance of the bead to the thermal velocity, represents the interaction time between DPD beads:

$$t^* = \frac{r^*}{v^*} = \sqrt{\frac{m_{(1)}[r^{\mathrm{c}}_{(1,1)}]^2}{[k_B T]}} \tag{48}$$

Although the thermal energy of the solvent is used as the scale for $k_B T$, since constant temperature is assumed in this model, it will make no difference to choose another temperature scale as k_B is a constant.

With these choices of scaling factors, the factor $v^* t^*/r^*$ in Equation (32) becomes identically equal to one. It should be noted that since Equations (32) and (33) are dimensionless, the groups of parameters that are formed in the process of non-dimensionalization have also to be dimensionless. Hence, the group $F^* t^*/m^* v^*$ in Equation (33) has to be dimensionless, and F^* must have the same dimensions as $m^* v^*/t^*$. Assuming this group equals one

$$F^* = \frac{[k_B T]}{r^{\mathrm{c}}_{(1,1)}} \tag{49}$$

Similarly, identifying the dimensionless groups for a^*, γ^* and σ^* in Equations (36), (38) and (40) and making the assumption that they are equal to one give the following factors:

$$a^* = F^* = \frac{[k_B T]}{r^{\mathrm{c}}_{(1,1)}} \tag{50}$$

$$\gamma^* = \frac{\sqrt{m_{(1)}[k_B T]}}{r^{\mathrm{c}}_{(1,1)}} \tag{51}$$

$$\sigma^* = \frac{[m_{(1)}]^{1/4}[k_B T]^{3/4}}{[r^{\mathrm{c}}_{(1,1)}]^{1/2}} \tag{52}$$

Equation (50) was also given by Maiti and McGrother [35] in a separate study. The factors γ^* and σ^* in Equations (51) and (52), respectively, reduce the FD relation in Equation (41) by making the group $[\gamma^*[k_B T]^*/[\sigma^*]^2]$ equal to one. The system volume is non-dimensionalized by the scaling factor for length, i.e. $\Omega^* = [r^*]^3$. Using the scaling parameter definitions from Equations (44)–(48), the force expressions in Equations (35)–(40) reduce to

$$\bar{\mathbf{F}}^{\mathrm{C}}_{i\alpha} = \sum_{\beta} \sum_{j\beta \neq i\alpha}^{N_\beta} \bar{\mathbf{f}}^{\mathrm{C}}_{i\alpha, j\beta} \tag{53}$$

$$\bar{\mathbf{f}}^{\mathrm{C}}_{i\alpha, j\beta} = \bar{a}_{\alpha,\beta} \bar{w}^{\mathrm{C}}_{i\alpha, j\beta}(\bar{r}_{i\alpha, j\beta})\, \hat{\bar{\mathbf{r}}}_{i\alpha, j\beta} \tag{54}$$

$$\bar{\mathbf{F}}^{\mathrm{D}}_{i\alpha} = -\sum_{\beta} \sum_{j\beta \neq i\alpha}^{N_\beta} \bar{\mathbf{f}}^{\mathrm{D}}_{i\alpha, j\beta} \tag{55}$$

DOI: 10.1002/fld

$$\bar{\mathbf{f}}^{\mathrm{D}}_{i\alpha,j\beta}=\bar{\gamma}_{\alpha,\beta}\bar{w}^{\mathrm{D}}_{i\alpha,j\beta}(\bar{r}_{i\alpha,j\beta})[\bar{\mathbf{v}}_{i\alpha,j\beta}\cdot\hat{\bar{\mathbf{r}}}_{i\alpha,j\beta}]\hat{\bar{\mathbf{r}}}_{i\alpha,j\beta} \tag{56}$$

$$\bar{\mathbf{F}}^{\mathrm{R}}_{i\alpha}=\sum_{\beta}\sum_{j\beta\neq i\alpha}^{N_\beta}\bar{\mathbf{f}}^{\mathrm{R}}_{i\alpha,j\beta} \tag{57}$$

$$\bar{\mathbf{f}}^{\mathrm{R}}_{i\alpha,j\beta}=\bar{\sigma}_{\alpha,\beta}\bar{w}^{\mathrm{R}}_{i\alpha,j\beta}(\bar{r}_{i\alpha,j\beta})\bar{\psi}_{i\alpha,j\beta}\,\mathrm{d}\bar{t}^{-1/2}\hat{\bar{\mathbf{r}}}_{i\alpha,j\beta} \tag{58}$$

where the general character of the equations in terms of components α and β is retained. With the above assumptions for scale factors, the expressions in Equations (53)–(58) reduce to Equations (3)–(4) given by Groot/Warren [34].

5. CHOICE OF PARAMETERS IN DPD

The main parameters in the dimensionless DPD equations are $\bar{a}_{\alpha,\beta}$, $\bar{\gamma}_{\alpha,\beta}$, $\bar{\sigma}_{\alpha,\beta}$, $\overline{k_BT}$ and $\Delta\bar{t}$, which have to be specified for the system. With the scaling factors defined in Section 4, the FD expression of Equation (41) reduces to

$$\bar{\sigma}^2_{\alpha,\beta}=2\bar{\gamma}_{\alpha,\beta}\overline{k_BT} \tag{59}$$

This expression relates three of the above parameters and hence only two need to be specified to calculate the third.

5.1. Conservative force parameter

In the original Groot/Warren model, the conservative force parameter for the solvent was set by matching the isothermal compressibility of the DPD solvent with that of water at 300 K. The inverse dimensionless isothermal compressibility $\kappa^{-1}_{(1)}$ of the solvent DPD beads is defined as

$$\frac{1}{[k_BT]}\left[\frac{\partial p}{\partial n}\right]_{(1)}=\kappa^{-1}_{(1)} \tag{60}$$

where n is the number of solvent particles in the volume Ω or $n=N^m_{(1)}N_{(1)}/\Omega_{(1)}=N^m_{(1)}\bar{\rho}_{(1)}/[r^{\mathrm{c}}_{(1,1)}]^3$ using Equation (31) for a single component. Using the scaling $p^*=k_BT/[r^{\mathrm{c}}_{(1,1)}]^3=F^*/[r^{\mathrm{c}}_{(1,1)}]^2$ and the definition of n from above, Equation (60) can be expressed in terms of dimensionless parameters as

$$\left[\frac{\partial\bar{p}}{\partial\bar{\rho}}\right]_{(1)}=N^m_{(1)}\kappa^{-1}_{(1)} \tag{61}$$

For water at 300 K, Keaveny *et al.* calculated $\kappa^{-1}_{(1)}=15.9835$ using MD simulations [39], which has also been reported by Groot/Warren [34] and Maiti and McGrother [35].

Groot/Warren and Maiti and McGrother obtained a simplified expression for the dimensionless pressure of a single component system:

$$\bar{p}_{(1)}=\bar{\rho}_{(1)}+c\bar{a}_{(1,1)}\bar{\rho}^2_{(1)} \tag{62}$$

DOI: 10.1002/fld

where all the beads in the single component system have the same conservative force parameter, which is denoted by a constant value of $\bar{a}_{(1,1)}$. The value of c was calculated to be 0.101 ± 0.001 to a good approximation for $\bar{\rho}_{(1)} > 2$ [34]. Using this equation for pressure, the inverse dimensionless isothermal compressibility of the DPD solvent in Equation (61) is matched with the value obtained numerically using MD to obtain the following expression for the intra-component conservative force parameter:

$$\bar{a}_{(1,1)} = \frac{[N^m_{(1)} \kappa^{-1}_{(1)}] - 1}{2c\bar{\rho}_{(1)}} \tag{63}$$

Maiti and McGrother have shown that the conservative force parameter for other components can be set by condition of mechanical equilibrium at the interface, i.e. the pressure in each component must be equal: $p_\alpha = p_{(1)}$. Since the form of the conservative force is soft repulsive, systems with finite surface tension between liquid and vapor phases, which need long-range attractive forces, cannot be modeled [34]. The equal pressure constraint leads to the following condition for the conservative intra-component parameter:

$$\frac{\bar{\rho}_{(1)}}{[r^c_{(1,1)}]^3} - \frac{\bar{\rho}_\alpha}{[r^c_{(\alpha,\alpha)}]^3} = c\left[\bar{a}_{(\alpha,\alpha)} \frac{\bar{\rho}^2_\alpha}{[r^c_{(\alpha,\alpha)}]^3} - \bar{a}_{(1,1)} \frac{\bar{\rho}^2_{(1)}}{[r^c_{(1,1)}]^3}\right] \tag{64}$$

In the case of polymer systems, the conservative inter-component parameter between the solvent and phase α: $\bar{a}_{(1),\alpha}$ is set based on the miscibility of the components. The free energy density in these systems is matched with the Flory–Huggins mean-field theory [40] to calculate the inter-component conservative force parameter from the χ parameter of polymer dynamics. The χ parameter controls whether the system will be well segregated or well mixed. In the case of a binary fluid system, the conservative force parameter can also be set based on a solubility parameter that is related to the Flory–Huggins χ parameter. The intra-component interactions in the Groot/Warren model were chosen to be the same for the solvent and phase α: $\bar{a}_{(1,1)} = \bar{a}_{(\alpha,\alpha)}$. This follows from Equation (64) provided that the bead volumes $\Phi_{(1)} = \bar{\rho}_{(1)}/[r^c_{(1,1)}]^3$, $\Phi_\alpha = \bar{\rho}_\alpha/[r^c_{(\alpha,\alpha)}]^3$ and the dimensionless densities $\bar{\rho}_{(1)}$, $\bar{\rho}_\alpha$ are assumed equal. This is consistent with the Flory–Huggins theory, which assumes that all the beads have to be of the same equilibrium volume. For this reason, the inter-component parameter $\bar{a}_{(1),\alpha}$ alone decides the chemistry of the system.

5.2. Dissipative and random force parameters

Unlike BD where the friction in the system is set based on the drag force experienced by the body, the friction parameter in DPD is heuristic in nature. In the original formulation by Groot/Warren, the dissipative and random force parameters were set empirically as a compromise between fast temperature equilibration, a fast simulation and acceptable numerical stability based on the velocity Verlet algorithm. The dissipative and random force parameters are also related via the FD theorem to the temperature of the system. A higher dissipation parameter in the system yields faster cooling, but can introduce numerical stability issues in the Groot/Warren algorithm. In this algorithm, the force evaluation is done only once per time step. This is insufficient if the friction parameter is set too high, as the dissipative and random forces will not be able to respond quickly enough to control the temperature. Groot/Warren recommend a dissipative parameter $\bar{\gamma}_{(1,1)} = 4.5$ and a random parameter $\bar{\sigma}_{(1,1)} = 3.0$ for a set temperature $\overline{k_B T} = 1.0$. Masters and Warren [41] who used Boltzmann pair collision theory to investigate the change in scaling behavior of viscosity, found

DOI: 10.1002/fld

that for $\bar{\gamma}_{(1,1)} \geqslant 5$ the velocity autocorrelation function deviates from the single exponential behavior and correlation effects start to take over early in the simulation. Visser *et al.* [42] suggest setting the intra-component friction based on the viscosity of the component and the inter-component friction based on lever rules. However, the application of this idea to real systems has yet to be investigated.

Table II. Values of DPD parameters and estimate of time scales in a typical single component simple fluid system based on water.

Number of molecules per bead: $N^m_{(1)}$	3
Dimensionless density: $\bar{\rho}_{(1)}$	3
Mass of molecule: $m^{\text{particle}}_{(1)}$	18 amu
Mass of bead: $m_{(1)}$ (Equation (4))	54 amu
Volume of molecule: $\Phi^{\text{particle}}_{(1)}$	30 Å^3
Volume of bead: $\Phi_{(1)}$ (Equation (5))	90 Å^3
Cut-off radius: $r^{\text{c}}_{(1,1)}$ (Equation (6))	6.463 Å
Temperature: T	300 K
Thermal velocity of bead: $v_{(1)}$ (Equation (47))	2.149 Å/ps
Dimensionless friction parameter*: $\bar{\gamma}_{(1,1)}$	4.5
Dimensionless noise parameter*: $\bar{\sigma}_{(1,1)}$	3.0
Dimensionless conservative force parameter†: $\bar{a}_{(1,1)}$	78.0
Scaling factor for friction parameter: γ^* (Equation (51))	18 amu/ps
Scaling factor for noise parameter: σ^* (Equation (52))	6.69×10^{-8} amu.Å/ps$^{3/2}$
Traversal time scale: t^* (Equation (48))	3.01 ps

*Groot/Warren [34].

†Groot and Rabone [16].

Table III. Ideal and simple fluid simulation parameters in DPD units.

Property	Ideal fluid	Simple fluid
N	3000	3000
$m^{\text{particle}}_{(1)}$	18 amu	18 amu
$\Phi^{\text{particle}}_{(1)}$	30 Å^3	30 Å^3
$N^m_{(1)}$	3	3
$\bar{m}_{(1)}$	1.0	1.0
$\bar{\rho}_{(1)}$	3	3
$\bar{\Omega}_{(1)}$	$10 \times 10 \times 10$	$10 \times 10 \times 10$
$\bar{r}^{\text{c}}_{(1,1)}$	1.0	1.0
$\bar{a}_{(1,1)}$	0.0	78.0
$\bar{\gamma}_{(1,1)}$	4.5	4.5
$\bar{\sigma}_{(1,1)}$	3.0	3.0
$\overline{k_B T}$	1.0	1.0
λ	0.65	0.65
$\Delta\bar{t}$	0.001–0.1	0.001–0.1

DOI: 10.1002/fld

5.3. System temperature

The system temperature is measured in dimensionless units of $[k_B T]^*$, the thermodynamic temperature. This temperature must in general be the same as the kinetic temperature that is obtained by inverting the expression in Equation (43) as isothermal DPD models systems at canonical equilibrium. In this case, the average dimensionless temperature $\overline{k_B T}$ must be the same for all components. This gives a new condition from the FD theorem in (59) that must be satisfied by all beads in the system for components α and β:

$$\frac{\bar{\sigma}_{\alpha,\alpha}^2}{\bar{\gamma}_{\alpha,\alpha}} = \frac{\bar{\sigma}_{\beta,\beta}^2}{\bar{\gamma}_{\beta,\beta}} = \frac{\bar{\sigma}_{\alpha,\beta}^2}{\bar{\gamma}_{\alpha,\beta}} \tag{65}$$

5.4. Time step

For physically meaningful simulations, the DPD time step $\Delta\bar{t}$ must be chosen smaller than the shortest characteristic time scales of the system. These time scales, discussed in detail by Ripoll *et al.* [38], are influenced by many factors including the thermal energy $\overline{k_B T}$ and the coarse-graining factor N^m. For example, Equations (4) and (5) show that an increase in N^m will cause increase in bead mass and bead volume. These changes decrease the diffusion constant and increase the time scales in the DPD system. Pivkin and Karniadakis [43] show that there are limits to the maximum value that N^m can take in both open and wall-bounded systems. Increase in coarse-graining beyond a critical value causes the DPD fluid to solidify, thereby changing the character of the solvent. In order to identify the appropriate DPD time step values to use with our multicomponent formulation, we investigate the effect of time step on the average system temperature for ideal, simple and binary fluid systems. This is done using the parameters in Tables II and III, which are based on a solvent of water at 300 K. Physically meaningful time steps are those that give calculated temperatures close to the 'set' temperature imposed on the system. These and other validation calculations are discussed in Section 6.

6. VALIDATION RESULTS AND DISCUSSION

The stochastic differential equations (32) and (33) can be integrated using various integration algorithms. In this paper we use the Groot/Warren [34] and self-consistent velocity Verlet [44] integrators to show the effect of time step on the temperature and radial distribution function (RDF). These results help to validate the simplified version of the multicomponent framework against existing results from the literature.

6.1. Temperature variation with time step

6.1.1. Ideal fluid. An ideal fluid system is one in which the conservative forces $\mathbf{F}^{\mathrm{C}}$ are absent. Although this system has no direct counterpart in real physical systems, it is useful for comparing with statistical mechanical theories and for understanding and benchmarking the effects of the dissipative and random forces on the system properties. Simulations on an ideal fluid system were performed for the set of parameters defined in Table III with periodic boundary conditions. The parameter λ in the table is the intermediate time step parameter used in the Groot/Warren integrator.

DOI: 10.1002/fld

The kinetic temperature of the system was calculated from the velocities using Equation (43) at every time step. The time-averaged temperature variation with time step is shown in Figure 1 for the Groot/Warren and self-consistent schemes for $\Delta\tilde{t}$ ranging from 0.001 to 0.1. At time steps less than 0.03 for the Groot/Warren integrator, the variation of actual kinetic temperature from the desired 'set' temperature $\overline{k_B T} = 1$ is less than 1%. For time steps 0.04 and 0.05, which have been used by Groot/Warren earlier, the variation is between 1 and 2%. The variation in the case of the self-consistent algorithm is roughly 3% at time steps greater than 0.05. In general, there is a positive drift with time step for the Groot/Warren integrator and a negative drift with time step for the self-consistent integrator. The trends and results match very well with simulations done by Groot/Warren and also by Vattulainen *et al.* [44]. For time steps greater than 0.5 (not shown), the Groot/Warren integration algorithm becomes highly unstable and the temperature reaches very high values. Error bars were calculated from the error of the mean (the ratio of standard deviation to the square root of number of time steps at which data is stored) and are so small as to be obscured by the points.

6.1.2. Simple fluid. A simple fluid system is one in which the conservative forces are included along with dissipative and random forces. The effect of the conservative force is to induce short-range repulsion in the system and hence it gives a non-zero pressure. The conservative force parameter for this system is set to $\bar{a}_{(1,1)} = 78.0$ following Groot and Rabone [16]. All other parameters are the same as that of the ideal fluid shown in Table III. The time-averaged temperature variation with time step is shown in Figure 2 for the Groot/Warren and self-consistent schemes.

The Groot/Warren algorithm shows an irregular variation in temperature with time step in the simple fluid case as compared with the ideal fluid, where it gradually increases. The self-consistent algorithm shows very steady temperatures with time step, although the temperature is about 2% lower than the desired value. For time steps of order 0.1 or greater (not shown) in the Groot/Warren

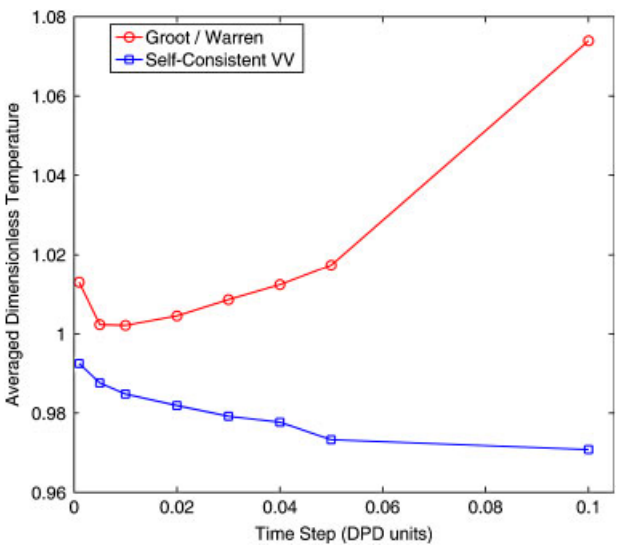

Figure 1. Variation of time-averaged dimensionless temperature with time step for ideal fluid system.

DOI: 10.1002/fld

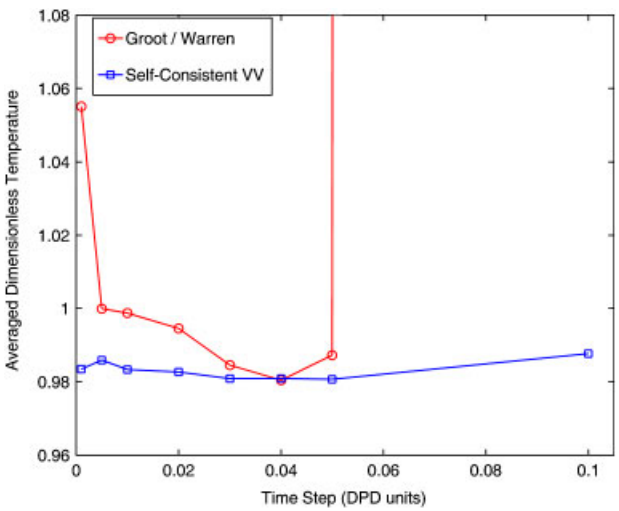

Figure 2. Variation of time-averaged dimensionless temperature with time step for the simple fluid system.

case, the temperature deviation is about two orders of magnitude. The self-consistent scheme is stable up to time steps of order 0.1. The error bars are again obscured by the points.

6.1.3. Binary fluid. The simplest extension of the above theory that can be made to a multicomponent system is the binary immiscible fluid. The idea is to check whether the temperature variation with time step also holds for such systems, as earlier studies on integrators and temperature variation focused primarily on single component systems. Addition of a second component changes the time and length scales and the force contributions, which must be accounted for by the integration algorithm. The system parameters chosen for this study are described in Table IV. All scaling factors in the system are based on the solvent fluid (1).

The choice of the inter-component conservative force parameter $\bar{a}_{(1,2)}$ is made so that the fluids are immiscible. This ensures that the χ parameter of the Flory–Huggins system is greater than 1 and that the system will phase segregate. From analysis of the fluid structure (Figures 8–10), the arbitrarily chosen value $\bar{a}_{(1,2)} = 120$ was found suitable to obtain immiscibility. The time-averaged temperature variation of the whole system with time step is shown in Figure 3 for both the integrators. The error bars are again obscured by the points. The temperature variation is similar to the Groot/Warren simple fluid case with both integrators breaking down at time steps of order 0.1 or greater. For the Groot/Warren integrator, the temperature variation for time steps less than 0.05 is within 2% of the desired temperature, whereas for the self-consistent case the variation is within 4% of the desired temperature. For small time steps of the order of 0.01 or less, the temperature variation is within 1% of the desired temperature.

6.2. Radial distribution function

The RDF $g(r)$ gives the average density as a function of distance from a given bead. The RDF is a good measure used to validate simulations by probing the structure of the DPD system and is calculated using the expression from [6]. From the center of the bead, the space around it is

DOI: 10.1002/fld

Table IV. Binary fluid simulation parameters in DPD units.

Property	Solvent fluid (1)	Suspended fluid (2)
N	2500	500
m^{particle}	18 amu	12 amu
Φ^{particle}	30 Å^3	30 Å^3
N^m	3	3
$\bar{m}$	1.0	0.67
$\bar{\rho}$	3.0	3.0
$\bar{\Omega}$	$10 \times 10 \times 10$	
$\begin{bmatrix} \bar{r}^{\text{c}}_{(1,1)} & \bar{r}^{\text{c}}_{(1,2)} \\ \bar{r}^{\text{c}}_{(2,1)} & \bar{r}^{\text{c}}_{(2,2)} \end{bmatrix}$	$\begin{bmatrix} 1.0 & 1.0 \\ 1.0 & 1.0 \end{bmatrix}$	
$\begin{bmatrix} \bar{a}_{(1,1)} & \bar{a}_{(1,2)} \\ \bar{a}_{(2,1)} & \bar{a}_{(2,2)} \end{bmatrix}$	$\begin{bmatrix} 78.0 & 120.0 \\ 120.0 & 78.0 \end{bmatrix}$	
$\begin{bmatrix} \bar{\gamma}_{(1,1)} & \bar{\gamma}_{(1,2)} \\ \bar{\gamma}_{(2,1)} & \bar{\gamma}_{(2,2)} \end{bmatrix}$	$\begin{bmatrix} 4.5 & 4.5 \\ 4.5 & 4.5 \end{bmatrix}$	
$\begin{bmatrix} \bar{\sigma}_{(1,1)} & \bar{\sigma}_{(1,2)} \\ \bar{\sigma}_{(2,1)} & \bar{\sigma}_{(2,2)} \end{bmatrix}$	$\begin{bmatrix} 3.0 & 3.0 \\ 3.0 & 3.0 \end{bmatrix}$	
$\bar{k_B T}$	1.0	
λ	0.65	
$\Delta\bar{t}$	0.001–0.1	
Traversal time scale: t^* (Equation (48))	3.01 ps (1 DPD unit)	2.46 ps (0.82 DPD units)

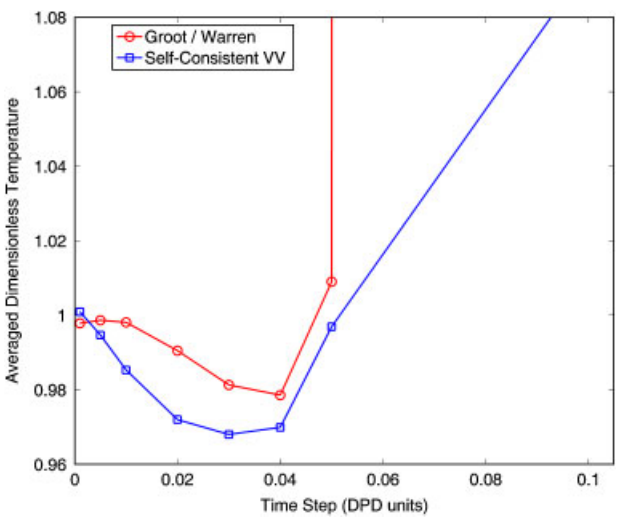

Figure 3. Variation of time-averaged dimensionless temperature with time step for binary fluid system.

divided into spherical shells (bins) and the number of beads in each bin is calculated. The ratio of the average number of beads per bin to the set number density, N/Ω, gives the RDF as it varies with distance away from the bead center.

DOI: 10.1002/fld

6.2.1. Ideal fluid. In the case of an ideal fluid, the RDF should be identically equal to one due to the absence of static correlations in the system. Figures 4 and 5 show the variation of time-averaged dimensionless RDF with time step ($\Delta\tilde{t}$) for the Groot/Warren and self-consistent integrators, respectively. Both integrators show artificial structure close to the particle, though it is more pronounced in the Groot/Warren case. The Groot/Warren integration scheme shows more structure due to the explicit nature of the algorithm. In the self-consistent scheme, the iterative process stabilizes the temperature that reduces the correlations close to the particle center. Another reason for the artificial structure is the size of the bins that can lead to numerical errors. These errors, given by the deviations of the simulation values from the true value of 1, decrease as one moves away from the bead center as seen in Figures 4 and 5.

6.2.2. Simple fluid. The time-averaged RDF for the simple fluid case is shown in Figure 6 for the Groot/Warren algorithm and Figure 7 for the self-consistent algorithm. Except for time steps of 0.1, the curves in Figure 6 are indistinguishable. The curve at 0.1 in Figure 6 is similar to that seen in the case of ideal fluid and indicates that the conservative force integration is not proper. At time steps of 0.1, the beads move longer distances in one step and hence increase the probability of inter-bead penetration. The physics of finite conservative force repulsion is not captured by the Groot/Warren algorithm at this time step. For the other time steps, a fluid-like character is shown by the distribution function. Close to the particle center the distribution function is zero due to finite repulsion. The curves in Figures 6 and 7 are only shown up to a distance of 1.0, which is the cut-off radius in the system. Away from the cut-off radius, the distribution function dips to the set density in the system, N/Ω and remains close to that value (one), as expected in a fluid. It should be noted from Figure 2 that at $\Delta\tilde{t}=0.1$, the temperature of the system is very high for the Groot/Warren scheme, which supplements the claim that time steps less than 0.1 are required with this integrator for a reasonable estimate of these properties.

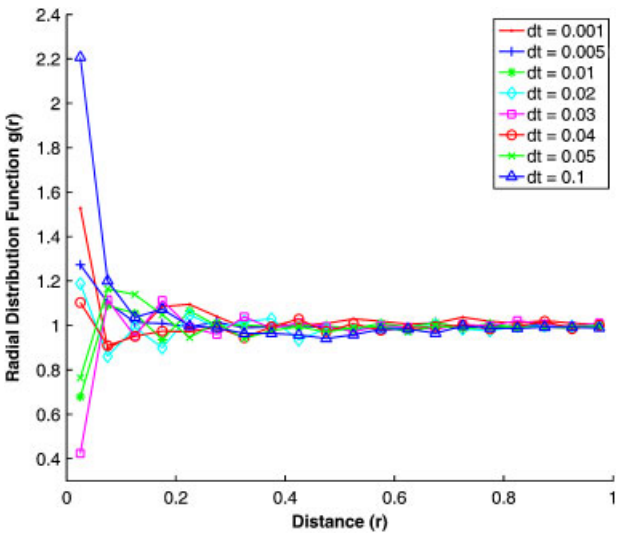

Figure 4. Dimensionless radial distribution function for the ideal fluid using the Groot/Warren integrator.

DOI: 10.1002/fld

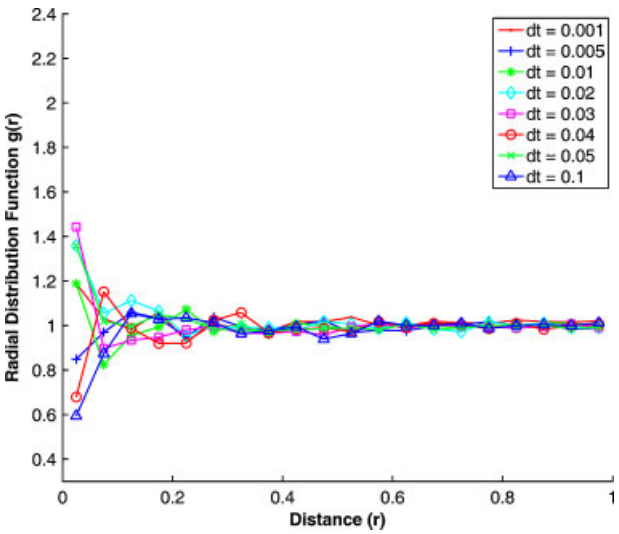

Figure 5. Dimensionless radial distribution function for the ideal fluid using the self-consistent integrator.

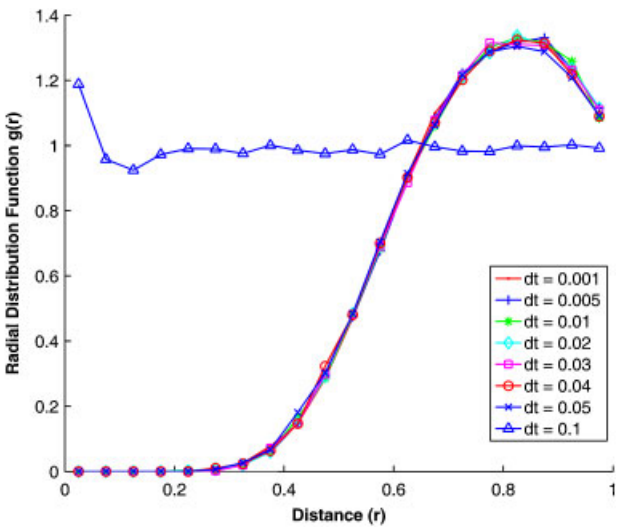

Figure 6. Dimensionless radial distribution function for the simple fluid using the Groot/Warren integrator.

Figure 7 shows the RDF for the self-consistent case, which suffers from similar problems for $\Delta\tilde{t}=0.1$. The trends observed at other time steps are very similar to that of the Groot/Warren case, which indicates that both integrators capture the essential physics very well for these time steps. Although the temperature conservation is good at a time step of 0.1, the RDF is not good. Hence, time steps smaller than 0.1 should be used to capture the physics of the system with the self-consistent integrator and obtain good temperature conservation.

DOI: 10.1002/fld

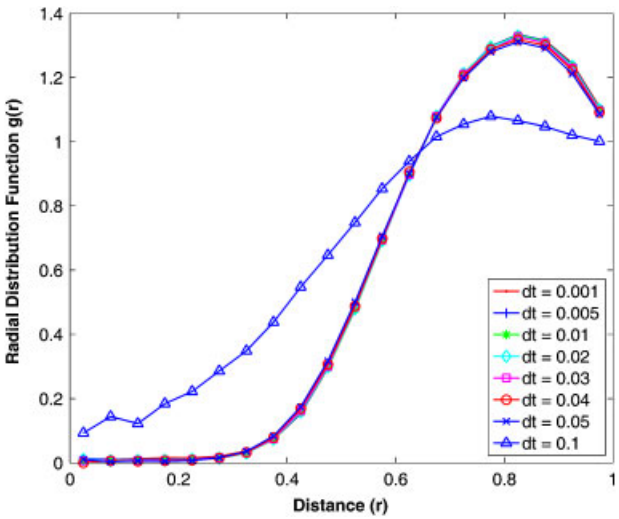

Figure 7. Dimensionless radial distribution function for the simple fluid using the self-consistent integrator.

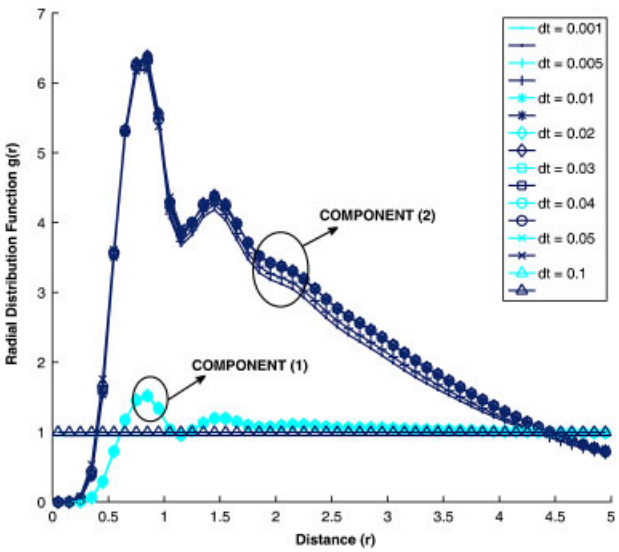

Figure 8. Dimensionless radial distribution function for the binary fluid using the Groot/Warren integrator.

6.2.3. Binary fluid. The intra-component RDF for both components of the binary fluid system is shown in Figures 8 and 9 for the Groot/Warren and self-consistent integrators, respectively. For the binary system the RDF for component α is found by finding the number of α beads per bin volume and dividing by the set density of component α, N_α/Ω. The values of N_α and Ω are found in the first line of Table IV. Both components show fluidic behavior with the characteristic crest at the location of the first nearest neighbors. The height of the crest in the case of the suspended

DOI: 10.1002/fld

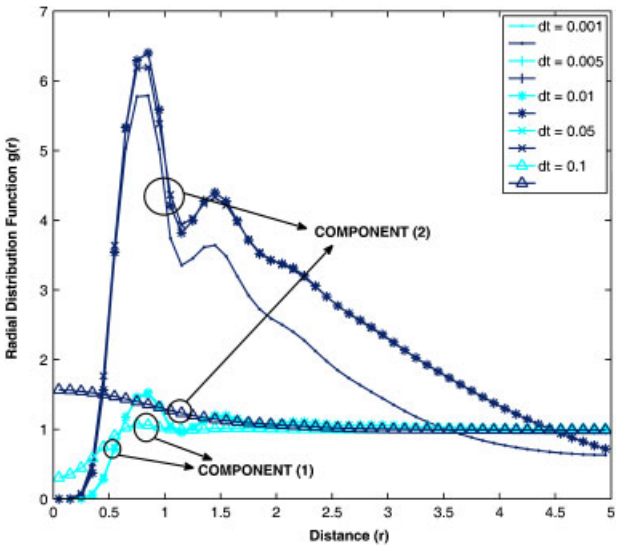

Figure 9. Dimensionless radial distribution function for the binary fluid using the self-consistent integrator.

fluid (2) is larger than that of the solvent fluid (1) because the RDF for (2) is normalized by a smaller number ($N_{(2)}/\Omega$) than for (1) ($N_{(1)}/\Omega$). The RDF for the solvent fluid (1) gradually settles at the value of one, which is the normalized set density for this fluid. The RDF for the suspended fluid (2), however, drops below one toward zero at larger values. This behavior arises due to phase segregation. The inter-bead repulsion between fluids (1) and (2) is very high, pushing the beads of (2) together and resulting in phase separation (Figure 10). At large enough distances from a given bead of (2), there will be no other beads of (2) as they are all concentrated into a single droplet rather than dispersed evenly throughout the system.

Figure 8 shows the RDF in the Groot/Warren case. Except for $\Delta\bar{t}=0.1$, all curves look similar. The ideal fluid-like behavior at $\Delta\bar{t}=0.1$ was also seen earlier in the simple fluid case and is due to the increase in inter-particle penetration with large time steps. Both fluid component RDFs show this behavior at $\Delta\bar{t}=0.1$. Figure 9 shows the RDF in the self-consistent case. Time steps in the range 0.02–0.04 have been omitted as the behavior is similar to that of the simple fluid case. The major difference between the Groot/Warren and this case is seen at $\Delta\bar{t}=0.001$, where the peak in the RDF for fluid (2) is notably lower than at other time steps. This could be due to errors in the self-consistent integration algorithm as compared with the Groot/Warren case. The algorithm breaks down at $\Delta\bar{t}=0.1$ as the RDF in Figure 9 shows the ideal fluid-like behavior similar to the Groot/Warren case.

7. CONCLUSIONS

In this paper, a complete multicomponent DPD framework has been presented for the first time. Initially, the general DPD equations are expressed in dimensional form. General scaling factors for time, length, velocity and mass are used to convert these equations to dimensionless form. Next, these scaling factors are explicitly defined in a manner consistent with DPD convention by

DOI: 10.1002/fld

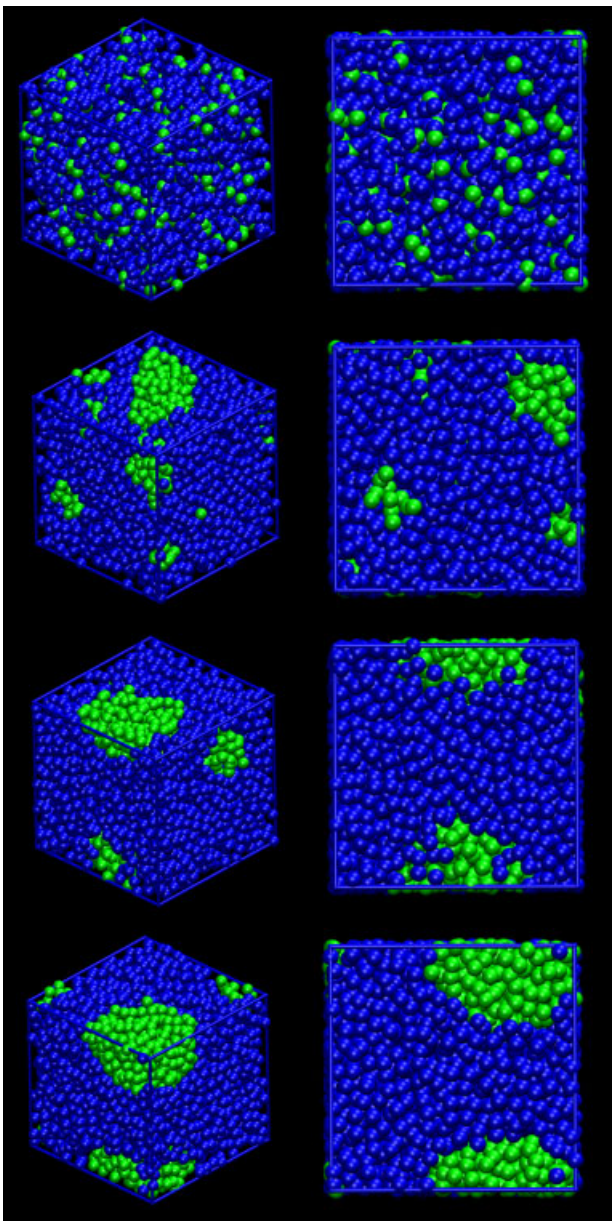

Figure 10. Phase segregation in a binary immiscible fluid system. Snapshots from top to bottom are in order of increasing time.

making use of solvent length and time scales. Explicit definition of these factors makes it possible to compute real dimensional physical properties with DPD simulations. The validation results for temperature variation with time step are in good agreement with the time scales of the system and with previously published results. The choice of the time step is limited by the shortest time scale

DOI: 10.1002/fld

and is based on the dissipative parameter in the system. This limit has been confirmed through the ideal and simple fluid simulations. The radial distribution function is a good indicator of the fluid-like behavior in the system and works very well for time steps less than 0.1. For time steps greater than 0.1 both Groot/Warren and self-consistent integrators break down and the simple fluid behavior changes to ideal fluid behavior. Simulation results for binary immiscible fluids show phase segregation as indicated by the radial distribution functions. The framework established here is an important step toward the practical application of multicomponent DPD for the analysis of complex fluid systems.

ACKNOWLEDGEMENTS

This work was partially supported by the Nano/Bio Interface Center, an NSF NSEC (DMR-0425780) and by the Office of Naval Research (grant no. N00014-07-1-0665).

REFERENCES

1. de Gennes PG. Soft matter. *Reviews of Modern Physics* 1992; **64**:645–648.
2. Gelbart WM, Ben-Shaul A. The 'New' science of complex fluids. *Journal of Physical Chemistry* 1996; **100**: 13169–13189.
3. Larson RG. *The Structure and Rheology of Complex Fluids* (*Topics in Chemical Engineering*). Oxford University Press: New York, 1999.
4. Crochet MJ, Walters K. Numerical methods in non-Newtonian fluid mechanics. *Annual Review of Fluid Mechanics* 1983; **15**:241–260.
5. Stickel JJ, Powell RL. Fluid mechanics and rheology of dense suspensions. *Annual Review of Fluid Mechanics* 2005; **37**:129–149.
6. Allen MP, Tildesley DJ. *Computer Simulation of Liquids*. Oxford University Press: New York, 1989.
7. Haile JM. *Molecular Dynamics Simulation*: *Elementary Methods*. Wiley-Interscience: New York, U.S.A., 1992.
8. Ermak DL, McCammon JA. Brownian dynamics with hydrodynamic interactions. *Journal of Chemical Physics* 1978; **69**:1352–1360.
9. Hoogerbrugge PJ, Koelman JMVA. Simulating microscopic hydrodynamic phenomena with dissipative particle dynamics. *Europhysics Letters* 1992; **19**:155–160.
10. Brady JF, Bossis G. Stokesian dynamics. *Annual Review of Fluid Mechanics* 1988; **20**:111–157.
11. Español P, Revenga M. Smoothed dissipative particle dynamics. *Physical Review E* 2003; **67**:026705-(1-12).
12. Succi S. *The Lattice Boltzmann Equation for Fluid Dynamics and Beyond*. Oxford University Press: U.S.A., 2001.
13. Rivet JP, Boon JP. *Lattice Gas Hydrodynamics*. Cambridge University Press: Cambridge, 2001.
14. Español P, Serrano M, Zuñiga I. Coarse-graining of a fluid and its relation with dissipative particle dynamics and smoothed particle dynamics. *International Journal of Modern Physics C* 1997; **8**:899–908.
15. Dzwinel W, Yuen DA. Matching macroscopic properties of binary fluids to the interactions of dissipative particle dynamics. *International Journal of Modern Physics C* 2000; **11**:1–25.
16. Groot RD, Rabone KL. Mesoscopic simulation of cell membrane damage, morphology change and rupture by nonionic surfactants. *Biophysical Journal* 2001; **81**:725–736.
17. Jakobsen AF, Mouritsen OG, Besold G. Artifacts in dynamical simulations of coarse-grained model lipid bilayers. *Journal of Chemical Physics* 2005; **122**:204901-(1-11).
18. Sugii T, Takagi S, Matsumoto Y. A meso-scale analysis of lipid bilayers with the dissipative particle dynamics method: thermally fluctuating interfaces. *International Journal for Numerical Methods in Fluids* 2007; **54**:831–840.
19. Yamamoto S, Maruyama Y, Hyodo S. Dissipative particle dynamics study of spontaneous vesicle formation of amphiphilic molecules. *Journal of Chemical Physics* 2002; **116**:5842–5849.
20. Gomes AE, Martins AF, Polimeno A. Dissipative particle dynamics approach to mesophase formation and behavior. *Molecular Crystals and Liquid Crystals* 2005; **435**:135–152.
21. Ortiz V, Nielsen SO, Discher DE, Klein ML, Lipowsky R, Shillcock J. Dissipative particle dynamics simulations of polymersomes. *Journal of Physical Chemistry B* 2005; **109**:17708–17714.

DOI: 10.1002/fld

22. Coveney PV, Novik KE. Computer simulation of domain growth and phase separation in two-dimensional binary immiscible fluids using dissipative particle dynamics. *Physical Review E* 1996; **54**:5134–5141.
23. Boek ES, Coveney PV, Lekkerkerker HNW, van der Schoot P. Simulating the rheology of dense colloidal suspensions using dissipative particle dynamics. *Physical Review E* 1997; **55**:3124–3133.
24. Maiti A, Wescott J, Kung P. Nanotube–polymer composites: insights from Flory–Huggins theory and mesoscale simulations. *Molecular Simulation* 2005; **31**:143–149.
25. Schlijper AG, Hoogerbrugge PJ, Manke CW. Computer simulation of dilute polymer solutions with the dissipative particle dynamics method. *Journal of Rheology* 1995; **39**:567–579.
26. Español P. Statistical mechanics of coarse-graining. *Novel Methods in Soft Matter Simulations*. Lecture Notes in Physics, vol. 605. Springer: Berlin, 2004; 69–115.
27. Gardiner CW. *Handbook of Stochastic Methods* (*for Physics*, *Chemistry and the Natural Sciences*) (3rd edn). Springer: Berlin, 2004.
28. Gillespie DT. *Markov Processes*: *An Introduction to Physical Scientists* (1st edn). Academic Press: New York, 1992.
29. Ross S. *A First Course in Probability*, vol. 1 (2nd edn). Macmillan: New York, 1984; 157.
30. Español P, Warren P. Statistical mechanics of dissipative particle dynamics. *Europhysics Letters* 1995; **30**:191–196.
31. Marsh CA, Backx G, Ernst MH. Static and dynamic properties of dissipative particle dynamics. *Physical Review E* 1997; **56**:1676–1691.
32. Marsh CA, Yeomans JM. Dissipative particle dynamics: the equilibrium for finite time steps. *Europhysics Letters* 1997; **37**:511–516.
33. Coveney PV, Español P. Dissipative particle dynamics for interacting multicomponent systems. *Journal of Physics A*: *Mathematical and General* 1997; **30**:779–784.
34. Groot RD, Warren PB. Dissipative particle dynamics: bridging the gap between atomistic and mesoscopic simulation. *Journal of Chemical Physics* 1997; **107**:4423–4435.
35. Maiti A, McGrother S. Bead–bead interaction parameters in dissipative particle dynamics: relation to bead-size, solubility parameter, and surface tension. *Journal of Chemical Physics* 2004; **120**:1594–1601.
36. Kundu PK, Cohen IM. *Fluid Mechanics* (4th edn). Academic Press: Amsterdam, 2008.
37. Munson BR, Young DF, Okiishi TH. *Fundamentals of Fluid Mechanics* (4th edn). Wiley: New York, 2002.
38. Ripoll M, Ernst MH, Español P. Large scale and mesoscopic hydrodynamics for dissipative particle dynamics. *Journal of Chemical Physics* 2001; **115**:7271–7284.
39. Keaveny EE, Pivkin IV, Maxey M, Karniadakis GE. A comparative study between dissipative particle dynamics and molecular dynamics for simple and complex geometry flows. *Journal of Chemical Physics* 2005; **123**:104107-(1-9).
40. Doi M, See H. *Introduction to Polymer Physics* (4th edn). Oxford University Press: Oxford, 2006.
41. Masters AJ, Warren PB. Kinetic theory for dissipative particle dynamics: the importance of collisions. *Europhysics Letters* 1999; **48**:1–7.
42. Visser DC, Hoefsloot HCJ, Iedema PD. Modeling multi-viscosity systems with dissipative particle dynamics. *Journal of Computational Physics* 2006; **214**:491–504.
43. Pivkin IV, Karniadakis GE. Coarse-graining limits in open and wall-bounded dissipative particle dynamics systems. *Journal of Chemical Physics* 2006; **124**:184101-(1-7).
44. Vattulainen I, Karttunen M, Besold G, Polson JM. Integration schemes for dissipative particle dynamics simulations: from softly interacting systems towards hybrid models. *Journal of Chemical Physics* 2002; **116**:3967–3979.

DOI: 10.1002/fld